Eur. Phys. J. B **5**, 45–52 (1998)

THE EUROPEAN PHYSICAL JOURNAL B

Ab initio calculation of elastic constants and electronic properties of ZnSe and ZnTe under uniaxial strain

J. Sörgel and U. Scherz[a]

Institut für Theoretische Physik, Technische Universität Berlin, Hardenbergstr. 36, 10623 Berlin, Germany

Received: 4 April 1998 / Accepted: 4 May 1998

Abstract. The second and third order elastic constants of ZnSe and ZnTe, the electronic deformation potentials, and other bulk properties under uniaxial strains are calculated. We used first-principles density-functional theory applied to supercells with the plane wave method and energy cutoffs of 30–40 Ry. The 3*d* states of Zn were treated as core states but a nonlinear core correction was used for the exchange and correlation energy. We determined the internal strain parameter and calculated the deformation density of unstrained ZnSe with and without Zn-3*d* valence states. The change of the electron density in ZnSe due to uniaxial strain in [001], [110], and [111] directions is demonstrated. We also present the density of states and the change of the deformation density of bulk ZnTe due to biaxial strain like in a thin epilayer on a GaAs(001) substrate. The change of the density of states is also discussed here. Finally, the Luttinger parameters of ZnSe are calculated.

PACS. 62.20.Dc Elasticity, elastic constants – 71.20.Nr Semiconductor compounds – 73.20.Dx Electron states in low-dimensional structures (superlattices, quantum well structures and multilayers)

1 Introduction

Large band-gap materials have attracted much attention in the last years because of a possible application for opto-electronic devices in the blue spectral region. Such systems are heterostructures of thin layers, which are stressed and strained due to the lattice-parameter mismatch. In order to analyse the crystal properties in composite devices, it is important to understand the elastic and electronic properties of crystals under biaxial strain [1,2].

We therefore performed first-principles calculations of cubic ZnSe and ZnTe crystals under uniaxial strain, as well as under biaxial strain, *e.g.* in a thin ZnTe epilayer on a GaAs substrate. We also calculated GaAs under uniaxial strain for a better comparison of our theoretical results, because a number of experimental and theoretical data were available for this material.

2 Theoretical method

2.1 Total energy calculations

Our calculations are based on the density-functional theory using the local density approximation [3,4]. The wave functions are expanded in plane waves with energy cutoffs in the range of 30–40 Ry. We used separable norm-conserving *ab initio* pseudopotentials after references [5–7]. For calculations with 3*d*-valence states for Zn, we generated Troullier-Martins pseudopotentials [8]. In the other cases the pseudopotentials are taken from reference [9], which are based on the pseudopotentials of reference [6]. The pseudopotential for Te is of the generalized Hamann type [10]. In the cases, in which we treat the Zn-3*d* states as core states, we use a nonlinear core correction [11]. The integration over the Brillouin zone was performed on grids of Monkhorst-Pack points [12]. The number of points was between 10 and 20, depending on the symmetry of the Brillouin zone. We used the computer program fhi93cp of the Fritz-Haber-Institut in Berlin [13].

2.2 Strain

We denote the location of a material point in an unstrained solid as $\boldsymbol{\xi} = (\xi_1, \xi_2, \xi_3)$ and its strained location as $\mathbf{x} = (x_1, x_2, x_3)$, and we describe the deformation as a mapping

$$\boldsymbol{\xi} \longrightarrow \mathbf{x}(\boldsymbol{\xi}), \tag{1}$$

which is defined for all points $\boldsymbol{\xi}$ of the solid. Then the deformation gradient $\underline{F} = \big(F_{ij}(\boldsymbol{\xi})\big)$

$$F_{ij}(\boldsymbol{\xi}) = \frac{\partial x_i(\boldsymbol{\xi})}{\partial \xi_j} \tag{2}$$

[a] e-mail: scherz@physik.tu-berlin.de

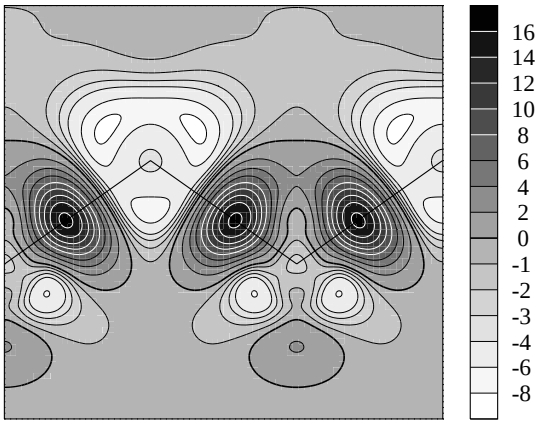

Fig. 1. Deformation density of ZnSe in 10^{-3} atomic units. The Zn $3d$ electrons are treated as core electrons. Shown is the (110) plane with the Zn atoms in the upper and the Se atoms in the lower positions of the zigzag line.

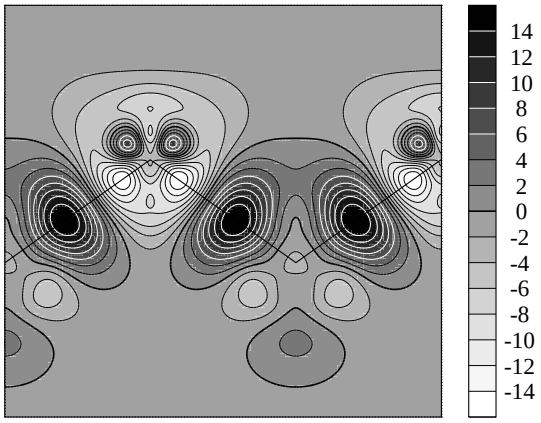

Fig. 2. Deformation density of ZnSe in 10^{-3} atomic units. The Zn $3d$ electrons are treated as valence electrons. Explanations as for Figure 1.

describes how vectors, which are tangential to lines s of material points, transform under the deformation:

$$\frac{d\mathbf{x}\big(\boldsymbol{\xi}(s)\big)}{ds} = \sum_{i=1}^{3} \left.\frac{\partial \mathbf{x}(\boldsymbol{\xi})}{\partial \xi_i}\right|_{\boldsymbol{\xi}(s)} \frac{d\xi_i(s)}{ds} = \underline{F}\big(\boldsymbol{\xi}(s)\big)\frac{d\boldsymbol{\xi}(s)}{ds}. \tag{3}$$

The strain tensor

$$\underline{\varepsilon} = \frac{1}{2}\big(\underline{F}^T\underline{F} - 1\big) \tag{4}$$

is used as usual as a measure for the strain. We do not linearise the strain tensor $\underline{\varepsilon}$ with respect to the shift field $\mathbf{x}(\boldsymbol{\xi})-\boldsymbol{\xi}$, in contrast to what is often done for small strains. This is necessary in order to properly describe the third order elastic constants, for which larger strains are considered.

3 Effect of 3d electrons

Lattice parameters are usually underestimated in pseudopotential calculations of II-VI semiconductors with Zn, when the cation $3d$ states are treated as core states. This effect can be explained by the anti-bonding character of the p-d-coupling [14], which is neglected in $3d$-core calculations. To demonstrate the different bonding properties of $3d$ electrons treated as core states or as valence states, we calculated the deformation density in both cases. The deformation density is the difference between the valence charge densities of the crystal and of the non-interacting neutral pseudoatoms. The deformation density therefore exhibits the change of the electron density due to chemical bonding. We used Troullier-Martins [8] pseudopotentials for Zn when dealing with the $3d$-valence states. Figures 1 and 2 show the contour plots of the resulting deformation densities. Since the $3d$ states are strongly localized at the zinc ions, we found considerable differences of the deformation density due to the $3d$ electrons in the neighbourhood of the zinc ions, especially we found charge depletion zones along the bonding axis, see Figure 2. The decrease of bonding charge weakens the screening of the charged Zn and Se ions. The result of this weaker screening is an increase of the bond length. We therefore obtained a higher and more correct lattice parameter of 5.619 Å in case of the $3d$ valence-electron calculation compared to the $3d$-core value of 5.496 Å, which is lower by 2.2%.

4 Elastic constants

We determined the second and third order elastic constants of ZnSe, ZnTe, and GaAs from total energy calculations by applying various uniaxial and biaxial strains described by the strain tensor $\underline{\varepsilon}$. The total energy per unit cell is thus interpreted as the strain energy density w. In cubic symmetry w is written in the form

$$\begin{aligned} w = {} & \frac{1}{2}c_{11}\big(\varepsilon_1^2+\varepsilon_2^2+\varepsilon_3^2\big) + c_{12}\big(\varepsilon_1\varepsilon_2+\varepsilon_1\varepsilon_3+\varepsilon_2\varepsilon_3\big) \\ & + \frac{1}{2}c_{44}\big(\varepsilon_4^2+\varepsilon_5^2+\varepsilon_6^2\big) + \frac{1}{6}c_{111}\big(\varepsilon_1^3+\varepsilon_2^3+\varepsilon_3^3\big) \\ & + \frac{1}{2}c_{112}\big(\varepsilon_1^2\varepsilon_2+\varepsilon_1\varepsilon_2^2+\varepsilon_1^2\varepsilon_3+\varepsilon_1\varepsilon_3^2+\varepsilon_2^2\varepsilon_3+\varepsilon_2\varepsilon_3^2\big) \\ & + c_{123}\varepsilon_1\varepsilon_2\varepsilon_3 + \frac{1}{2}c_{144}\big(\varepsilon_1\varepsilon_4^2+\varepsilon_2\varepsilon_5^2+\varepsilon_3\varepsilon_6^2\big) \\ & + \frac{1}{2}c_{155}\big(\varepsilon_2\varepsilon_4^2+\varepsilon_3\varepsilon_4^2+\varepsilon_1\varepsilon_5^2+\varepsilon_3\varepsilon_5^2+\varepsilon_1\varepsilon_6^2+\varepsilon_2\varepsilon_6^2\big) \\ & + c_{456}\varepsilon_4\varepsilon_5\varepsilon_6. \end{aligned} \tag{5}$$

In case of the elastic constants c_{44}, c_{144}, c_{155} and c_{456}, the applied homogeneous strain is accompanied by an additional internal strain in form of a relative shift of the two sublattices of the two ion species. The direction of the internal strain is determined by symmetry: the uniaxial [110] strain leads to an internal strain in [001] direction and for the [111] strain in the [111] direction. We determine the amount of the relative shift of the two sublattices from the minimum of the total energy.

For simplicity the strain tensor is often linearised with respect to the deformation gradient. This approximation, however, is restricted to small strains and we did not use it for a correct treatment of the large strains necessary to describe the third order elastic constants. The results of our calculations are listed in Tables 1 and 2 together with experimental and theoretical data from various authors.

We conclude from Table 1 that it is necessary to take the internal strain into account. This is also important for the third order elastic constants, for which we obtained $c_{144} = -248\,\mathrm{GPa}$ for ZnSe without internal strain instead of $-64\,\mathrm{GPa}$ by taking internal strain into account. The figures for c_{155} are $-337\,\mathrm{GPa}$ instead of $-131\,\mathrm{GPa}$ and for c_{456} $-290\,\mathrm{GPa}$ instead of $-64\,\mathrm{GPa}$ respectively.

The calculated values of c_{11} and c_{44} for ZnSe and ZnTe are slightly too large compared with the experiments. This may be a consequence of the neglect of the Zn-3d valence states. As discussed in Section 3, the use of Zn-3d core electrons results in overestimated bonding forces, which lead to overestimated elastic constants. This effect, however, is not seen at c_{12}. Our third order elastic constants of ZnSe and ZnTe differ significantly from the results of Prasad [26], which is the only measurement known to us.

5 Internal strain parameter

We use the internal strain parameter ζ as introduced by Kleinman [30] for zincblende-type crystals. Let $\mathbf{u}$ be the internal strain vector which shifts one sublattice relative to its unshifted position and $\mathbf{u}_0$ the (unphysical) internal strain vector which shifts the second sublattice in a position so that the nearest neighbour bond lengths are unchanged with respect to the unstrained crystal [31]. In our case $\mathbf{u}$ and $\mathbf{u}_0$ are parallel and ζ is then given by $\mathbf{u} = \zeta\mathbf{u}_0$.

We examined three uniaxial strains in [001], [110], and [111] directions. Their deformation gradients are denoted by $\underline{F}_1$, $\underline{F}_2$, and $\underline{F}_3$, and are given by

$$\underline{F}_1 = \begin{pmatrix} \sqrt{1-2\delta^2} & \delta & \delta \\ \delta & \sqrt{1-2\delta^2} & \delta \\ \delta & \delta & \sqrt{1-2\delta^2} \end{pmatrix}$$
$$\underline{F}_2 = \begin{pmatrix} 1+\delta & \delta & 0 \\ \delta & 1+\delta & 0 \\ 0 & 0 & 1 \end{pmatrix} \qquad (6)$$
$$\underline{F}_3 = \begin{pmatrix} 1+\delta & \delta & \delta \\ \delta & 1+\delta & \delta \\ \delta & \delta & 1+\delta \end{pmatrix}.$$

Here δ describes the amount of the uniaxial strain, with $\delta > 0$ in case of expansion and $\delta < 0$ in case of compression. Our results for the internal strain parameter ζ as a function of δ are shown in Figure 3 for GaAs and in Figure 4 for ZnSe. The decrease of ζ with increasing δ is due to the weakening of bonding with increasing bond length.

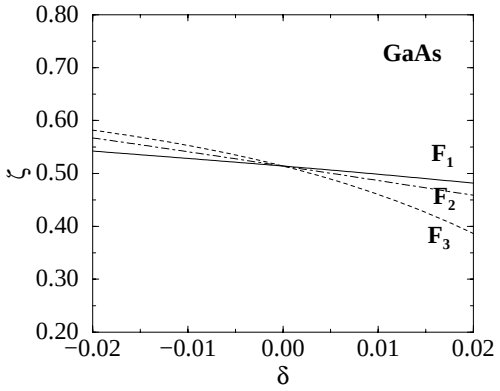

Fig. 3. Internal strain parameter ζ as a function of the amount δ of the applied uniaxial strain for GaAs. Here $\delta < 0$ means compression and $\delta > 0$ means expansion.

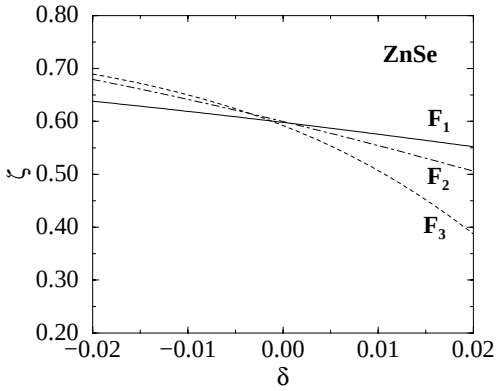

Fig. 4. Internal strain parameter ζ as a function of the amount δ of the applied uniaxial strain for ZnSe.

The resulting internal strain parameters ζ for $\delta = 0$ are compared in Table 1 with published experimental and theoretical data. Our results for GaAs agree within 3% or 7% to two newer measurements of references [21] and [22]. There are no measurements or *ab initio* calculations of ζ for ZnSe or ZnTe known to us. The results of Martin [18], who used a valence force model, are about 15–18% higher compared to our *ab initio* calculations.

6 Deformation potentials

The shift and splitting of the electronic band structure can be described in first order by deformation potentials [32]. We calculated the deformation-potential parameters a_{gap}, b and d from the Kohn-Sham band structure, see reference [33]. It can be seen from Table 3 that a_{gap} is underestimated by 10-30% compared to the experimental data, *i.e.* the measured increase of the bandgap caused by an increasing hydrostatic pressure is smaller. This is due to the well known band-gap problem of the density-functional theory in the local density approximation, because the conduction band edge is not occupied in our calculation. The deformation potential parameters b and d, however, describe the splitting of the valence-band edge under specific tetragonal or trigonal strains. Because only

Table 1. Second order elastic constants in GPa and internal strain parameter ζ. The superscript zero at c_{44} indicates that the calculation is done without taking the internal strain into account. The experimental values of c_{11}, c_{12} and c_{44} are extrapolated to zero temperature. VFM denotes a valence-force model used in reference [18].

		c_{11}	c_{12}	c_{44}	c_{44}^0	ζ
ZnSe	this work	97.8	52.5	47.0	63.1	0.596
	exp. [15]	94.3	57.3	41.35		
	exp. [16]	88.8	52.7	41.4		
	exp. [17]	82.8	46.2	41.2		
	VFM [18]					0.723
ZnTe	this work	81.5	42.0	37.4	50.1	0.580
	exp. [16]	73.7	42.3	32.1		
	VFM [18]					0.706
GaAs	this work	125.6	55.06	60.56	79.4	0.514
	exp. [19]	121.07	54.77	60.36		
	exp. [20]	122.6	57.1	60.0		
	exp. [21]					0.55 ± 0.02
	exp. [22]					0.53
	theor. [23]					0.517
	theor. [24]					0.528 ± 0.002
	theor. [25]					0.48
	VFM [18]					0.600

Table 2. Third order elastic constants in GPa.

		c_{111}	c_{112}	c_{123}	c_{144}	c_{155}	c_{456}
ZnSe	this work	−620	−359	−98	−64	−131	−64
	exp. [26]	−827	−136	−551	+222	−265	−278
ZnTe	this work	−492	−301	−87	−81	−139	−36
	exp. [26]	−707	−121	−412	+183	−217	−229
GaAs	this work	−600	−401	−94	+10	−305	−43
	exp. [27]	−675	−402	−4	−70	−320	−69
	exp. [28]	−622	−387	−57	+2	−269	−39
	exp. [29]	−620	−392	−62	+8	−274	−43

Table 3. Relative deformation potentials in eV.

	GaAs			ZnSe			ZnTe		
	a_{gap}	b	d	a_{gap}	b	d	a_{gap}	b	d
this work	−9.80	−1.97	−4.67	−6.37	−1.33	−4.12	−6.17	−1.36	−4.32
	−8.1	−1.7	−4.4	−4.4	−1.0	−3.8		−1.2	
exp.	to	to	to	to	to	to	−5.5	to	−4.3
	−9.0	−2.1	−6.0	−5.8	−1.3	−6.1		−1.4	
Refs. [34,35]	−7.2		−4.54	−6.7			−5.3		
Ref. [36]		−2.07			−1.37				

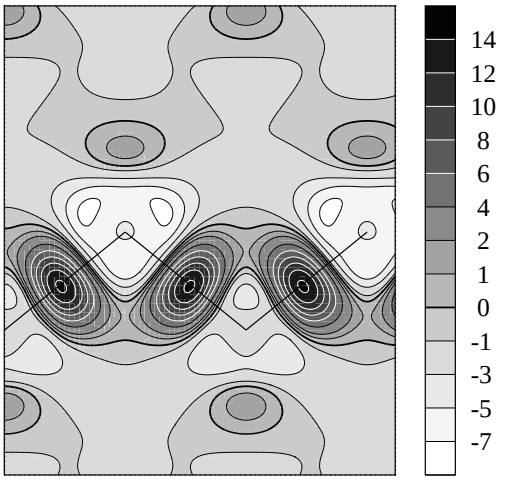

Fig. 5. Deformation density of ZnTe in the (110) plane strained like a thin layer on a GaAs(001) substrate. Units are 10^{-3} atomic units. The Zn atoms are in the upper and the Te atoms in the lower positions of the zigzag line.

occupied states are involved here, our results for b and d are within or near the intervals built up from various experimental values.

7 ZnTe strained like in a layer on a GaAs(001) substrate

We calculated the deformation density and the density of states of bulk ZnTe strained like a pseudomorphic ZnTe epilayer on a GaAs(001) substrate. We assumed a perfect interface, *i.e.* we considered a homogeneously strained ZnTe crystal due to the lattice mismatch between ZnTe and GaAs and neglected the interface reconstruction. The atomic spacings in the ZnTe layer parallel to the interface are assumed to be equal to those in the perfect GaAs substrate, and we calculated the relaxation of the ZnTe layer perpendicular to the interface from the minimum of the total energy. The resulting deformation density in the (110) plane of ZnTe is shown in Figure 5. Figure 6 shows the difference between the deformation density of Figure 5, projected to the unstrained coordinates, and the deformation density of the unstrained ZnTe crystal. This difference exhibits the response of the valence electrons to the applied strain. The most striking feature in Figure 6 is the concentration of charge above and below the zinc ions in the upper positions of the zigzag line. A possible explanation for this is the larger overlap of the bonding charge between two neighbouring ions. If the two ions belong to bonding chains which are oriented in [110] direction, as shown in Figure 6, or in the $[\bar{1}10]$ direction, the strain reduces the angle between two neighbouring bonds and the overlap of the bonding charge increases. There is no corresponding concentration of charge above and below the Te ions, although the bonding angle decreases here too. The biggest charge depletion zones in Figure 6 are located at the left and right sides of the zinc ions.

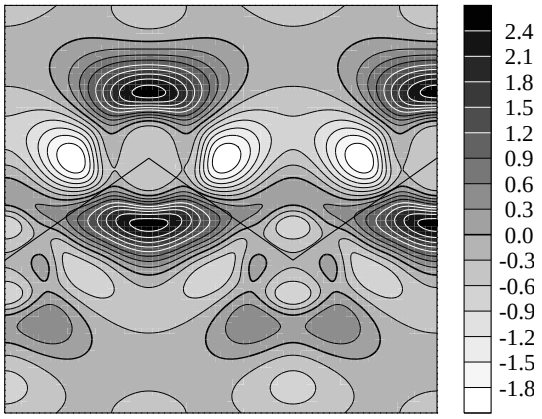

Fig. 6. Difference of the deformation densities of ZnTe strained like in Figure 5 and of the unstrained crystal. The deformation density of the strained crystal has been projected to the corresponding unstrained coordinates. Explanations as for Figure 5.

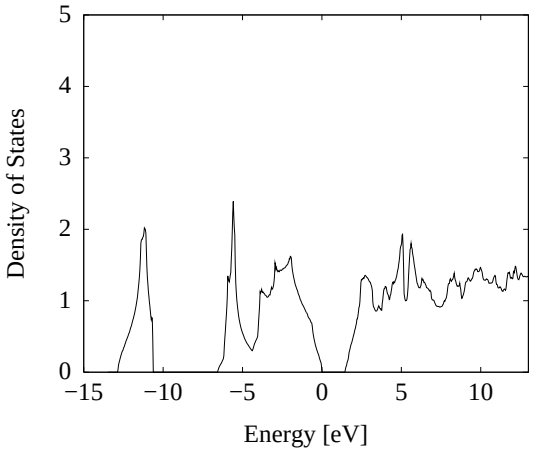

Fig. 7. Density of states of ZnTe strained like in a thin layer on a GaAs(001) substrate. Shown is the density of states in units of number of states per unit cell and per eV.

The density of states (DOS) of ZnTe, as in the ZnTe/GaAs(001) structure, is shown in Figure 7 and can be compared with the DOS of unstrained ZnTe in Figure 8. The slope of the valence band edge in the strained DOS is smaller than without strain, which is a consequence of the splitting of the valence band. The two highest peaks (upper edge of the lowest band and lower edge of second lowest band) are lower in the DOS of the strained crystal. This indicates that the band structure close to the two band edges is not so flat for the strained crystal. In addition, the two highest peaks of the DOS of the strained crystal are at lower energies with respect to the upper valence band edge (zero energy) compared with the unstrained crystal.

8 Change of the electron density due to uniaxial strain

In order to demonstrate the response of the valence electrons to uniaxial strain in ZnSe, we calculated the

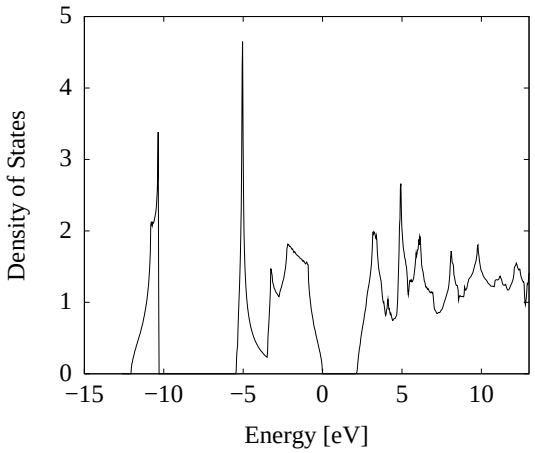

Fig. 8. Density of states of the perfect ZnTe crystal in units of number of states per unit cell and per eV.

deformation densities of the strained and of the unstrained crystal. Both densities can be compared by subtracting one from the other, if the deformation density of the strained crystal is projected with respect to the coordinates of the unstrained crystal. There is, however, a complication in case of internal strain, because the atomic positions of the two deformation densities are not the same. We therefore did not subtract the deformation density of the unstrained crystal, but of a crystal with an appropriate pure internal strain. Such a pure internal strain is not accompanied by an external homogeneous strain, but can be regarded as an optical phonon at the Γ point.

We examined three volume conserving uniaxial strains in [001], [110], and [111] directions, which correspond to the following deformation gradients

$$\underline{F}_{[001]} = \frac{1}{(1+\delta)^{1/3}} \begin{pmatrix} 1 & 0 & 0 \\ 0 & 1 & 0 \\ 0 & 0 & 1+\delta \end{pmatrix}$$

$$\underline{F}_{[110]} = \frac{1}{(1+2\delta)^{1/3}} \begin{pmatrix} 1+\delta & \delta & 0 \\ \delta & 1+\delta & 0 \\ 0 & 0 & 1 \end{pmatrix} \qquad (7)$$

$$\underline{F}_{[111]} = \frac{1}{(1+3\delta)^{1/3}} \begin{pmatrix} 1+\delta & \delta & \delta \\ \delta & 1+\delta & \delta \\ \delta & \delta & 1+\delta \end{pmatrix}.$$

The values for δ were chosen so that the crystal is stretched by 6% in the corresponding directions. The calculated differences of the deformation densities of the strained and of the unstrained crystal are shown in Figures 9–11. Figure 9 is qualitatively similar to Figure 6 because the point symmetry group D_{2d} is the same for the ZnSe crystal, strained in [001] direction, and the ZnTe crystal strained like a thin layer on a GaAs(001) substrate. The strain in [110] direction, described by $\underline{F}_{[110]}$ of equation (7), causes charge depletion zones near the middle of the bonding axes, see Figure 10. This may be due to the increase of bond length which results in a decrease of the electronic screening of the positively charged ions. In case of the uniaxial strain in

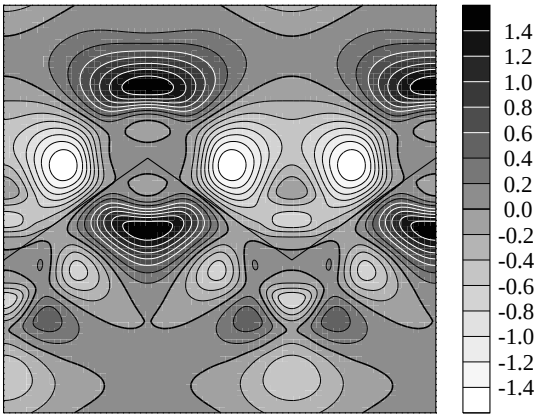

Fig. 9. Difference between the deformation densities of a ZnSe crystal strained in the [001] direction and of the unstrained crystal. The corresponding deformation gradient $\underline{F}_{[001]}$ is given in equation (7). Units are 10^{-3} atomic units. Shown is the (110) plane with the Zn atoms in the upper and the Se atoms in the lower positions of the zigzag line.

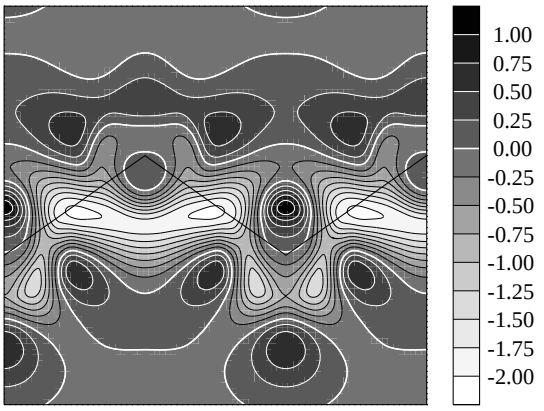

Fig. 10. Difference between the deformation densities of a ZnSe crystal strained in the [110] direction and of the unstrained crystal. Explanations as for Figure 9.

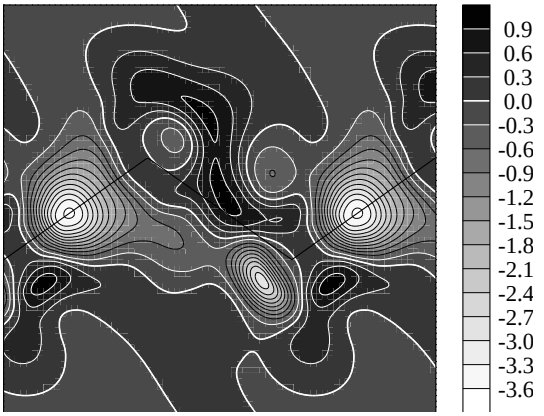

Fig. 11. Difference between the deformation densities of a ZnSe crystal strained in the [111] direction and of the unstrained crystal. Explanations as for Figure 9.

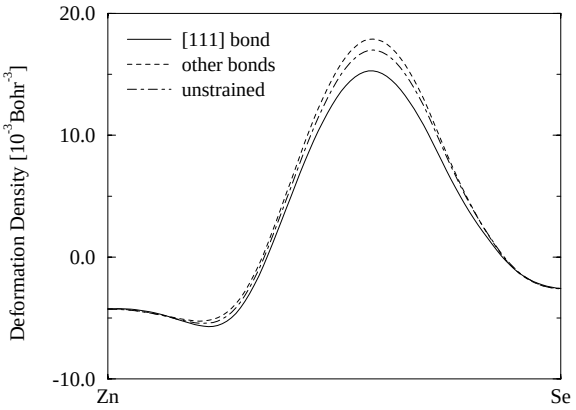

Fig. 12. Deformation density of a ZnSe crystal, strained in the [111] direction, along the bond length. The solid curve is for a bond in [111] direction and the dashed curve for the other bonds. The dot dashed curve is for an unstrained crystal. For a better comparison, the bond lengths are resized in the figure to the bond length of the unstrained crystal. Units are 10^{-3} atomic units.

Table 4. Luttinger parameters for ZnSe. The experimental values of reference [39] were taken at 4.2 K.

	γ_1	γ_2	γ_3
this work	2.786	0.676	1.025
exp. [39]	2.45(5)	0.61(12)	1.11(10)
exp. [40]	4.30	1.14	1.84

[111] direction, Figure 11 shows remarkably strong depletion zones near the center of the bonds in [111] direction, which is stretched most compared to the other bonds.

In the case of $\underline{F}_{[111]}$ the change of the deformation density due to uniaxial strain is plotted in Figure 12 along the bond length for a better quantitative comparison. It can be seen that the charge flows off the bond, which lies in the stretching direction, whereas the other bonds gain charge.

9 Luttinger parameters of ZnSe

We derived the Luttinger parameters for ZnSe by fitting the *ab initio* band structure of the three upper valence bands close to the Γ-point to the band structure of a simple one-level $3 \times 3 -$ kp model. By doing this, we obtain the three Dressselhaus parameters [37], which can be related to the Luttinger parameters [38], by assuming a weak spin-orbit coupling [32] in ZnSe. The results are listed in Table 4.

The low temperature values, obtained from two-photon magneto absorption [39], agree within 8–13% with our calculations. This indicates that the shape of the valence-band edge is correctly described by our method. The data of reference [40] are obtained by Rutherford back scattering.

10 Discussion

We have presented complete sets of third order elastic constants of ZnSe, ZnTe and GaAs. The comparison of the values of GaAs with data from several experiments demonstrates that our method is suitable to describe third order effects correctly. For ZnSe and ZnTe there is a strong deviation between our third order elastic constants and those of Prasad [26], the only experimental values known to us. The internal strain must be included in the calculation, in order to obtain correct values for the elastic constants c_{44}, c_{144}, c_{155} and c_{456}. As far as we know, the internal strain parameter for ZnSe and ZnTe were neither measured nor calculated with *ab inito* methods so far. Our values are 15–18% below those of Martin [18], who used a simple valence-force model.

The comparison of the deformation density of unstrained ZnSe, with and without the Zn-3d valence states, visualizes the influence of the Zn-3d states on the bonding properties. The Zn-3d states reduce the deformation density in a region along the Zn-Se bond axis near the Zn ion. This effect weakens the ion screening, and therefore weakens the bonding forces.

The comparison of the deformation density of a strained ZnTe layer in an ideal ZnTe/GaAs(001) heterostructure with that of unstrained ZnTe gives us an insight in the rearrangement of the valence electrons due to the tetragonal strain in the thin layer. The main feature here is a charge accumulation above and below the Zn ions in the [001] direction, which is perpendicular to the interface.

The deformation potentials, which are related to the valence band only (parameters b and d), are well reproduced for all three materials, while a_{gap} is underestimated by 10–30% due to the band-gap problem of the density-functional theory. The shape of the valence band near the band edge for ZnSe is correctly described by our Kohn-Sham band structure. This can be concluded from the agreement between our Luttinger parameters and the experimental values.

We are grateful to Prof. Dr. M. Scheffler for valuable discussions and his permanent interest in this work. We thank the Zentraleinrichtung Rechenzentrum of the Technische Universität Berlin and the Konrad-Zuse-Zentrum für Informationstechnik Berlin for their support and the provision of computing facilities.

References

1. D. Fröhlich, W. Nieswand, U.W. Pohl, J. Wrzesinski, Phys. Rev. B **52**, 14652 (1995).
2. F. Kubacki, J. Gutowski, D. Hommel, M. Heuken, U.W. Pohl, Phys. Rev. B **54**, 2028 (1996).
3. D.M. Ceperley, B.J. Alder, Phys. Rev. Lett. **45**, 5566 (1980).
4. J. Perdew, A. Zunger, Phys. Rev. B **23**, 5048 (1981).
5. D.R. Hamann, M. Schlüter, C. Chiang, Phys. Rev. Lett. **43**, 1494 (1979).

6. G.B. Bachelet, D.R. Hamann, M. Schlüter, Phys. Rev. B **21**, 4199 (1982).
7. L. Kleinman, D.M. Bylander, Phys. Rev. Lett. **48**, 1425 (1982).
8. N. Troullier, J.L. Martins, Phys. Rev. B **43**, 1993 (1990).
9. R. Stumpf, X. Gonze, M. Scheffler, *A List of Separable, Norm-conserving, ab initio Pseudopotentials* (1993), Fritz-Haber-Institut research report, (unpublished).
10. D.R. Hamann, Phys. Rev. B **40**, 2980 (1989).
11. S.G. Louie, S. Froyen, M.L. Cohen, Phys. Rev. B **26**, 1738 (1981).
12. H.J. Monkhorst, J.D. Pack, Phys. Rev. B **13**, 5188 (1976).
13. R. Stumpf, M. Scheffler, Comp. Phys. Commun. **79**, 447 (1994).
14. S.-H. Wei, A. Zunger, Phys. Rev. B **37**, 8958 (1987).
15. V.I. Kuskov, A.P. Rusakov, A.N. Mentser, Sov. Phys. Solid State **14**, 1869 (1973).
16. B.H. Lee, J. Appl. Phys. **41**, 2984 (1970).
17. Y.A. Burenkov, A.A. Botaki, S.Y. Davydov, S.P. Nikanorov, Sov. Phys. Solid State **19**, 1595 (1977).
18. R.M. Martin, Phys. Rev. B **1**, 4005 (1970).
19. R.I. Cottman, G.A. Saunders, J. Phys. C **6**, 2105 (1973).
20. C.W. Garland, K.C. Park, J. Appl. Phys. **33**, 760 (1962).
21. C.S.G. Cousins, L. Gerward, J. Staun Olsen, B. Selsmark, B.J. Sheldon, G.E. Webster, J. Semicond. Sci. Technol. **4**, 333 (1989).
22. E. Anastassakis, M. Cardona, Solid State Commun. **64**, 543 (1987).
23. J.E. Reynolds, Z.H. Levine, J.W. Wilkins, Phys. Rev. B **51**, 10477 (1995).
24. S. de Gironcoli, S. Baroni, R. Resta, Phys. Rev. Lett. **62**, 2853 (1989).
25. O.H. Nielsen, R.M. Martin, Phys. Rev. B **32**, 3792 (1985).
26. O.H. Prasad, Ph.D. thesis, Osmania University, Hyderabat 1978.
27. J.R. Drabble, A.J. Brammer, Solid State Commun. **4**, 467 (1966).
28. H.J. McSkimin, P. Andreatch, J. Acoust. Soc. Am. **34**, 609 (1967).
29. Y. Abe, K. Imai, Jpn. J. Appl. Phys. **25**, Suppl. 25-1, 67 (1986).
30. L. Kleinman, Phys. Rev. **128**, 2614 (1962).
31. For strains, which do not possess a bond length conserving internal strain, $\mathbf{u}_0$ means the internal strain vector leading to a minimum change in bond length.
32. G.L. Bir, G.E. Pikus, *Symmetry and Strain-Induced Effects in Semiconductors* (Wiley, New York, 1974).
33. J. Sörgel, Ph.D. thesis, Technical University of Berlin, 1995.
34. M. Cardona, N.E. Christensen, Phys. Rev. B **35**, 6182 (1987); B **36**, 2906 (1987).
35. N.E. Christensen, Phys. Rev. B **30**, 5753 (1984).
36. A. Qteish, R.N. Needs, Phys. Rev. B **43**, 4229 (1991).
37. G. Dresselhaus, A.F. Kip, C. Kittel, Phys. Rev. B **98**, 368 (1955).
38. J.M. Luttinger, Phys. Rev. B **102**, 1030 (1956).
39. H.W. Hölscher, A. Nöthe, C. Uihlein, Physica B **117-118**, 395 (1983).
40. B. Sermage, G. Fishman, Phys. Rev. B **23**, 5107 (1981).